Quantifying hydraulic roughness from field data: can dune morphology tell the whole story?

S.I de Lange[1], S. Naqshband[1], A.J.F. Hoitink[1]

[1]Wageningen University, Department of Environmental Sciences, Hydrology and Quantitative Water Management, Wageningen, the Netherlands

Key Points:

- Roughness predictions based on bedform geometry explain about half of the variance in friction factors inferred from water surface profiles
- Metrics capturing dune leeside angle statistics do not outperform classical hydraulic roughness predictors in explaining friction variation
- Bed level gradients oscillate in counter phase with the friction factor, indicating the importance of multi-kilometer depth variation

Corresponding author: Sjoukje de Lange, sjoukje.delange@wur.nl

Abstract

Hydraulic roughness is a fundamental property in river research, as it directly affects water levels, flow strength and the associated sediment transport rates. However quantification of roughness is challenging, as it is not directly measurable in the field. In lowland rivers, bedforms are a major source of hydraulic roughness. Decades of research has focused on dunes to allow parameterisation of roughness. This study aims to establish the predictive capacity of current roughness predictors, and to identify reasons for the unexplained part of the variance in roughness. We quantify hydraulic roughness based on the Darcy-Weisbach friction factor calculated from hydraulic field data of a 78 km long trajectory of the Lower Rhine and River Waal in the Netherlands. This is compared to predicted roughness values based on dune geometry, and to the spatial distribution of the local topographic leeside angle, both inferred from bathymetric field data. Results from both approaches show the same general trend and magnitude of roughness values (friction factor f=0.019-0.069, mean 0.035). Roughness inferred from dune geometry explains 42% of the variance, for the best performing predictor. Efforts to explain the remaining variance from statistics of the local topographic leeside angles, which supposedly control flow separation, were unsuccessful. Unexpectedly, multi-kilometer depth oscillations explain 34% of the total roughness variations. We suggest that flow divergence associated with depth increase causes energy loss, which is reflected in an elevated hydraulic roughness. Depth variations occur in many rivers worldwide, which may imply a cause of flow resistance that needs further study.

Plain Language Summary

Hydraulic roughness is the resistance that a river flow experiences from the bed and banks of the channel. Studying hydraulic roughness aids in the prediction of flooding, as increased resistance causes the water level to rise. Previous research on hydraulic roughness has mainly focused on the shape of river dunes at the river bed. Dunes interact with water flow, which has been captured in many equations predicting roughness. In this study, we tested several of those equations, and examined why they do not always work well. A 78 km-long segment of the Lower Rhine and River Waal in the Netherlands was used as a case study. Hydraulic roughness was inferred from longitudinal water surface level profiles measured with a survey vessel, and also from river dune dimensions. Both methodologies showed similar values and the same general trend of roughness, however, river dune dimensions only explained about half of the total observed variation. We found that, contrary to expectations, multiple-kilometer long fluctuations of the river bed elevation influence roughness as well. As the river deepens, the flow slows, increasing roughness in that region. This is an important finding, since many rivers feature such multi-kilometer depth variation.

1 Introduction

Hydraulic roughness, which quantifies the resistance to flow by objects protruding into the water flow (Chow, 1959), is a fundamental property in hydraulics. By influencing among others water level, flow structure and the associated sediment transport, understanding roughness is crucial to comprehend river dynamics. Quantification of hydraulic roughness is challenging, since it is not directly measurable in the field.

In lowland rivers, typically, bedforms are the major cause of form roughness (Julien et al., 2002; Gates & Al-Zahrani, 1996). The shape of the river bed, featuring bars, dunes, and ripples, influence the resulting roughness variations. Despite the existence of many hydraulic roughness predictors based on dune geometry, roughness coefficients in numerical models are often calibrated based on measured water levels and discharges. Unfortunately, these calibrated values are only valid for the conditions used for calibration (Klemes, 1986). For improvement of operational models, it is essential to identify and quantify

the spatiotemporal roughness variation, yet geographical insight about roughness is limited.

Hydraulic roughness at the bed of a main channel with abundant bedforms consists of form drag and friction drag. Predictors based on dune height and length estimate the form drag induced by bedforms (Bartholdy et al., 2010; Lefebvre & Winter, 2016; Soulsby, 1997; Van Rijn, 1984). Many (semi-) empirical equations are adjusted versions of the empirical roughness model of Van Rijn (1984) (Soulsby, 1997; Bartholdy et al., 2010), and are mainly calibrated on flume data. Unlike many others (Warmink, 2011; Engelund & Hansen, 1967), the predictor of Van Rijn (1984) is also calibrated on field data, and the predictor by Lefebvre and Winter (2016) is based on numerical experiments. Unfortunately, the predictive value of those equations is often limited (Warmink et al., 2013), and there is a large variation in predicted roughness among alternative formulations (Warmink, 2011).

The limited predictive value can be attributed to two things. First, hydraulic roughness is, just like bed shear stress, scale dependent (Vermeulen et al., 2013). In other words, roughness from a point measurement will be different from roughness integrated over a dune field, over a cross-section, or over a longitudinal transect (Buschman et al., 2009; Hoitink et al., 2009; Sassi et al., 2011; Hidayat et al., 2011). Roughness predictors are often empirical equations derived from laboratory flume studies and are based on an integration over 2D dunes in a dune field, without limited consideration of scale-dependency.

Secondly, relations drawn under laboratory conditions are translated to field situations by nondimensionalizing the results. Recent research has shown that dunes in flumes have a too high steepness and leeside angle, which causes more flow separation than in field conditions (Lefebvre & Winter, 2016; Cisneros et al., 2020; Kostaschuk & Venditti, 2019). The nondimensional slip face angle, at the steepest part of the leeside, and the relative dune height determine the strength of the flow separation zone (Cisneros et al., 2020; Best & Kostaschuk, 2002), and hence determine the total form roughness (Lefebvre et al., 2013). Relations drawn under laboratory conditions are therefor not directly applicable to field conditions and may lead to considerable uncertainties in model outcome (Warmink, 2011).

In many lowland rivers, the bathymetry is measured regularly to control the navigation depth. These elevation models are a potential source of knowledge for roughness induced by the river bed. Regular bathymetric measurements can identify spatiotemporal dynamics of bedforms, and disclose information about dune geometry such as its leeside angle. For example, recent research of de Ruijsscher et al. (2020), shows that dune geometry is dependent on its location on alternating river banks.

The aim of this paper is to establish the predictive capacity of well-established roughness predictors, and to identify reasons for the unexplained part of the variance in estimated roughness. We will do this based on discharge information, multibeam surveys, and water surface slope measurements over a trajectory of 78 kilometer of the main branch of River Rhine in the Netherlands. Ultimately, this could be used to improve roughness quantification in operational models, such as an state of the art operational model of the Rhine branches in the Netherlands (Rijntakkenmodel) (RWS-WVL & Deltares, 2017).

The remainder of this paper is structured as follows. Section 2 offers details about the field site subject to study. In section 3, the methods are described, which provides details of the roughness predictors we evaluate. Section 4 documents the results, which reveals that estimates of roughness inferred from the measured surface level profiles are coherent with the slope of bars in the river. Section 5 offers a discussion on the results, and in section 6, conclusions are drawn.

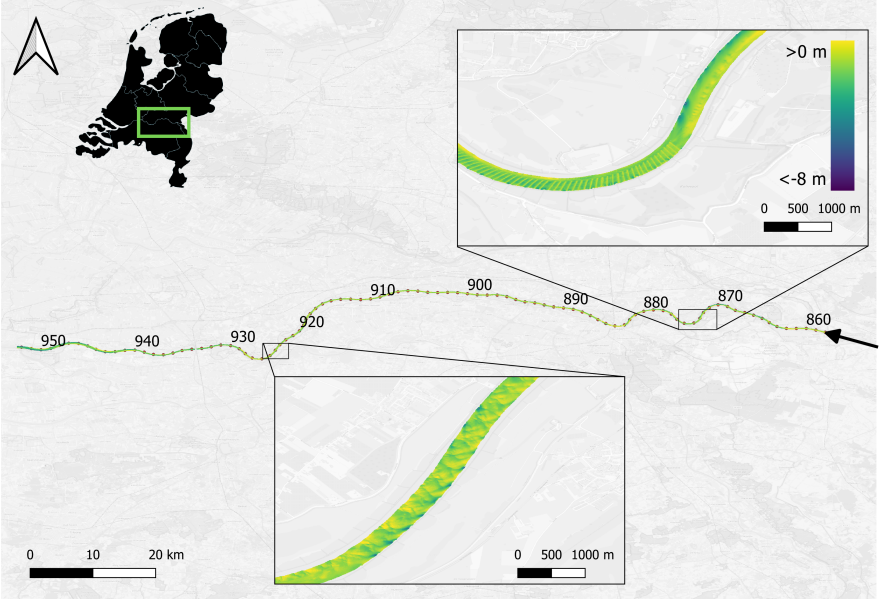

Figure 1. Overview of the study area from river kilometer 857 to 935, the Lower Rhine and its main branch river Waal in the Netherlands. Flow direction is from right to left. Each of the indicated place names has a gauging station. Inserts show local bathymetry (below) and human interference by hard layers of boulders in the shape of sine waves on the river bed (above).

2 Field site

The lowland sand bedded part of the river Rhine and its main distributary, the River Waal, are the venue of our research. The upper Rhine enters the Netherlands at Lobith and bifurcates into two branches at the Pannerdense Kop (Figure 1). We focus on the reach between the city of Lobith, where the river Rhine crosses the Dutch border, until the location where the tidal motion starts to influence the water levels (city of Zaltbommel). This reach is 78 km long (river kilometer km 857 - 935; Figure 1) and along this reach the river changes from a relatively course to a fine sand bedded river (Figure 6A).

The discharge entering the Netherlands at Lobith is on average 2300 m^3s^{-1}, but can fluctuate significantly between 800 and 12,000 m^3s^{-1} during a high discharge event in 1995 (Schielen et al., 2007). If the discharge exceeds 4000 m^3s^{-1}, floodplains convey part of the discharge. The main branch, the River Waal, receives about two third of the water discharge measured at Lobith (Schielen et al., 2007).

The course of the river Waal is strongly influenced by artificial structures including groynes. The groynes extend 40 - 80 m into the main channel and are on average spaced 200 m apart (Yossef, 2004). Between river kilometer 912 and 921, longitudinal training dams (LTDs) were constructed in 2014 and 2015 (de Ruijsscher et al., 2020), replacing the groynes in the inner bends of the river. They split the river in a main channel and two bank-connected side channels of approximately 90 m wide. Most field measurements were taken during the construction of the LTDs, and care should be taken when comparing data in this region from different months. Around Nijmegen (km 883-885) and St. Andries (km 925-928) fixed non-erodible layers in the outer bend (with a width of approximately 150 m) are constructed (Sloff et al., 2006), and at Erlecom (km 873-876) an artificial hard layer in the shape of a sine with a wavelength of 50 m fixes the bed.

An on average 3 m deep and 500 m long scour hole has developed downstream of these hard layers, and backwater raises water levels upstream. Therefore, the regions with a fixed bed are excluded in our current analysis.

The width of the summer bed between the groynes varies between 220 and 350 m, and generally increases in downstream direction. Bars and river dunes exist on multiple scales (de Ruijsscher et al., 2020; Zomer et al., 2021) and differences in dune dimensions are mainly caused by differences in grain size and discharge distribution (Wilbers & Ten Brinke, 2003). Just like dunes, the hydraulic roughness varies spatiotemporally (RWS-WVL & Deltares, 2017; Julien et al., 2002). Characteristics of this reach of the river Waal are summarized in Table 1.

Table 1. Characterisics, discretized per kilometer, of the Upper Rhine and River Waal in the Netherlands, between Lobith and Zaltbommel. *local variation is smoothed with an 8km LOESS filter, see Section 3.1.5 for explanation of variables. ** excluding bank connected side channel behind longitudinal training dams.

	symbol	unit	mean	max	min	std
large scale bed slope*	S_0	-	$1.01\ 10^{-4}$	$1.90\ 10^{-4}$	$1.53\ 10^{-4}$	$2.63\ 10^{-5}$
large scale pressure slope*	S_p	-	$-1.93\ 10^{-5}$	$0.42\ 10^{-4}$	$-1.721\ 10^{-3}$	$3.31\ 10^{-5}$
width conducting section**	W	m	276.3	346.2	222.4	35.1
water depth	d	m	4.52	5.57	3.45	0.41
discharge	Q	m^3/s	1030.4	1664.2	772.4	82.5
flow velocity	u	m/s	0.84	1.06	0.44	0.12

3 Methods

First, the collection and preprocessing of field data used for determining hydraulic roughness is discussed. Then, we explain how we infer hydraulic roughness from water surface slopes. This is followed by methods for roughness prediction based on dune characteristics along a longitudinal profile. This is used to discuss the predictive capacity of selected roughness predictors. Then, a method to derive leeside angle statistics is discussed. In the last section, the coefficient of determination is introduced, which we use to assess how much of the variance in hydraulic roughness is explained by dune roughness predictors and leeside angle statistics.

Field data is collected between 2014 and 2016 during periods of low river discharge, varying between 781 and 1353 m^3/s at Tiel (Table 2).

3.1 Data availability and preprocessing

3.1.1 Water level and discharge

Gauging stations (at each indicated place name in Figure 1) continuously record 10-minute averages of the water level (h). Water level is recorded with reference to the Amsterdam Ordnance Datum. Water level and discharge data are made available by the Dutch Ministry for Infrastructure and Environment, Rijkswaterstaat (RWS), and can be downloaded from their website (waterinfo.rws.nl). RWS calculates discharges at Lobith, Pannerdense Kop and Tiel via a multistation rating curve. To correct for simplifications made in this rating curve, 267 direct Acoustic Doppler Current Profiler measurement surveys from 2015 till 2017 are used to calculate a correction factor per location (see section 3.1.5).

Three water surface slope profiles from Lobith till Vuren are measured in June and August 2015 and October 2016, corresponding with a river discharge of 1270, 880 and 781 m^3s^{-1}, respectively (Table 2). The water level is measured with a sensor mounted at the outside of the vessel at the water level. The average deviation between the measured water level with the sensor and the gauging stations is 0.11 m, 0.08 m and 0.02 m respectively, which is used to correct the water surface slope profiles. Fluctuations of water level during a measurement campaign due to slowly changing water level during the measurement time, are in the order of a few centimeters, and are disregarded. Water surface slope profiles are measured during relatively low discharge conditions. This assures that only discharge takes place in the summer bed and roughness imposed by the floodplains will not influence the water surface slope. Simultaneous with the water surface slope measurements, a singlebeam echosounder (SBES) scanned the underlying bathymetry along the same line. Corresponding multibeam echosounding (MBES) measurements are conducted separately on part of this transect, from Dodewaard to Zaltbommel.

Table 2. Overview of data. x, y, z data from MBES campaings. Two MBES campaigns have an additional local topographic leeside angle γ measured. Pressure slope (S_p) is derived from water surface slope measurements, with additional SBES bed level measurements taken at the same time.

field data	start date	discharge at Tiel (m^3/s)	measurement reach (river km)
x, y, z, γ	22/9/14	1249	857 - 952
x, y, z, γ	20/10/14	1353	857 - 952
x, y, z	6/7/15	1271	895 - 936
x, y, z	5/8/15	880	895 - 936
x, y, z	12/10/16	781	895 - 936
Sp, z	6/7/15	1271	857 - 952
Sp, z	5/8/15	880	857 - 952
Sp, z	12/10/16	781	857 - 952

3.1.2 Multibeam echosounding

Data from a multibeam echosounder (MBES) is gridded onto a 1x1 m^2 grid. Only grid cells with a minimum 10 hits per m^2 are analyzed, but in general a much larger number of data points is collected per cell. The resulting five MBES datasets contain x, y and z coordinates. For two datasets an additional processing step is performed, where a surface is fitted through the grid cell, resulting in an additional value for slope and orientation per grid cell. These two special campaigns contain data from Lobith until Vuren, measured in September 2014 and October and November 2014, over the whole river width. The average discharge at Tiel during the field measurements was 1249 m^3s^{-1} and 1353 m^3s^{-1} respectively (Table 2). The surveys took approximately two weeks, wherein the river discharge was relatively constant. The discharge differences at the start and end of the surveys were 157 and 104 $m^3\ s^{-1}$, respectively.

The remaining three MBES datasets are taken at around the same date as the water surface slope measurements (section 3.1.1) and only comprise of x, y and z coordinates without the additional processing step for slope and orientation. They are limited to river kilometer 895 through 936 (Table 2).

Next, all bed level data is converted from Cartesian (x, y) coordinates to curvilinear coordinates (s, n) with the same spatial resolution (Vermeulen et al., 2014). Herein s is the longitudinal direction, parallel to the river, and corresponds with river kilometres. n is the cross-sectional direction, wherein $n = 0$ m is defined as the central river

axis, which roughly coincides with the thalweg. Besides transformation of the x, y-coordinates, the vector rotation of the cells was calculated to transform the orientation of the fitted surface to along river direction.

3.1.3 Grain size

Grain size samples are taken in 2020 with a Hamon Happer, in which the upper 25 cm of the river bed is taken. The samples are taken at every 500 m at the center line, and subsequently analysed with seive sizes between 63 um and 90 mm (Reneerkens, 2020). From this the 50^{th} and 90^{th} percentile (D50 and D90) are calculated.

3.1.4 Determining river geometry from field data

River geometry is here parameterized by river width, cross-sectional area, curvature and transverse bed slope. Man-made structures fixes the river width and curvature to near-constant values, however cross-sectional area is dependent on water level. River width W (m) is determined from a polygon following the longitudinal river outline though the groyne heads, and is taken constant over time. Under low discharge conditions, such as in this study, this measure is considered to be the discharge carrying section of the river. Assuming a trapezoidal shaped channel with a top width W, where the measured water depth represents the width averaged water level, and the slope of the groynes is 1/3, the cross-sectional area A (m^2) can be calculated. Curvature r (km^{-1}) is defined as the inverse of bend radius, following the approach of de Ruijsscher et al. (2020). Finally, transverse bed slope ξ (-) is defined as the slope between the two sides of the summer bed, longitudinally discretised in parts of 50m.

3.1.5 Determining hydraulic parameters from field data

The water surface surveys (see section 3.1.1), give an high resolution profile (on average approximately 400 samples per km) of water level h (m) and bed level z (m) over the central axis. The water depth d (m) is calculated by subtracting the bed level z from the water surface level h. The bed level is calculated from the corresponding bed level measurements, taken simultaneously with the water surface measurements. We choose to use bed level measurement from the simultaneously taken SBES measurements, since the corresponding MBES measurements are not available over the full length of the study area. The validity of this procedure is checked by constructing a filtered width-averaged bed level from these three MBES surveys and comparing this with the filtered SBES profiles in the part of the study area where there is data available from both datasets. The datasets show a very comparable large scale bed level profile, hence the use of the SBES dataset will not influence the analysis.

River discharge Q ($m^3\ s^{-1}$) at Lobith, Pannerdense Kop and Tiel is calculated via a multistation rating curve, and is subsequently corrected with a correction factor derived from Acoustic Doppler Current Profiler measurements (a fifth degree polynomial fit; see supplementary information Figure S1). The discharge at Tiel is generally underestimated (up to 15 %) while at Lobith, the rating relations can overestimate the discharge up to 10 %. Discharge is set constant between Lobith and the Pannerdense Kop since no major confluences or bifurcations occur. From there until Tiel, discharge is assumed to decrease or increase linearly due to several small supply and drainage channels. From Tiel until Zaltbommel, discharge is considered to be constant. At the section of the LTDs, approximately 12 percent of the discharge is conveyed by the bank connected side channels (Ruijsscher et al., 2019; Sieben, 2020). Width averaged flow velocity u (m/s) is determined by dividing discharge in the main channel by cross-section between the groynes.

3.2 Roughness inferred from water surface slopes

We estimate the Chézy coefficient directly from field measurements according to:

$$C = \frac{u}{\sqrt{d(S_0 - S_p - \frac{\partial Qu}{\partial s}\frac{1}{gA})}} \tag{1}$$

where u = depth-width averaged flow velocity (m/s), s = along river distance (m), d = water depth (m), S_0 = bottom slope (= ∂z/∂s, in which z = bed level relative to NAP, m), S_p = pressure slope (= ∂d/∂s), Q is discharge (m^3 s^{-1}) and A is cross-sectional area (m^2). Appendix A offers a derivation of equation 1.

All input parameters are discretized per kilometer, after smoothing with an 8km LOESS filter (de Ruijsscher et al., 2018; Cleveland, 1979; Cleveland & Devlin, 1988). This span is chosen to be the best trade-off between accuracy and resolution of the Chézy coefficient (see supplementary information Figure S2). From the Chézy coefficient, we calculate the dimensionless Darcy-Weisbach friction factor according to (Silberman et al., 1963):

$$f = \frac{8g}{C^2} \tag{2}$$

where g = gravitational acceleration (m s^{-2}).

3.3 Roughness inferred from dune characteristics

Existing roughness predictors based on dune characteristics including length (λ), height (Δ) and leeside angle (ϕ) were used to determine form roughness. Those characteristics were determined using a well-established BTT (Van der Mark & Blom, 2007), following the methodology described in de Ruijsscher et al. (2020).

The MBES bed elevation data was initially detrended by subtracting a reference surface from the Dutch national water authority based on the minimum depth of the fairway, established for dredging. An along river profile was constructed at the central river axis, and from this, bedform characteristics were determined. A filter span c = 1/6 was chosen to filter out small features. Two bedform lengths of interest are defined (Zomer et al., 2021): 5m ±5 (hereafter referred to as superimposed bedforms) and 100m ±30 (hereafter referred to as dunes), and the corresponding span values (P0) are used as input for detrending the profile (Figure 2). The span values are based on a spectral analysis to determine the dominant wave lengths in each section. The bedform lengths of interest (estimated bedform length) is also an input parameter for the smoothing of the profile. Based on the zero-crossings profile, dune characteristics are described every kilometer. We only consider the three characteristics which are used in the roughness prediction equations: dune height Δ (m), i.e. the vertical distance between top and downstream trough, dune length λ (m), i.e. the horizontal distance between two subsequent crests, and leeside angle ϕ (°), obtained from a linear fit of the leeside of the dune, excluding the upper and lower 1/6 of the dune height. Dune steepness Δ/λ can be inferred from this.

Form roughness (f_f) imposed by dunes, can be predicted employing several previously developed equations, which commonly require dune height and length as input. Van Rijn (1984) developed an equation based on calibration of field and lab data.

$$f_f = \frac{8g}{(18\log(\frac{12d}{k_s}))^2} \tag{3}$$

in which

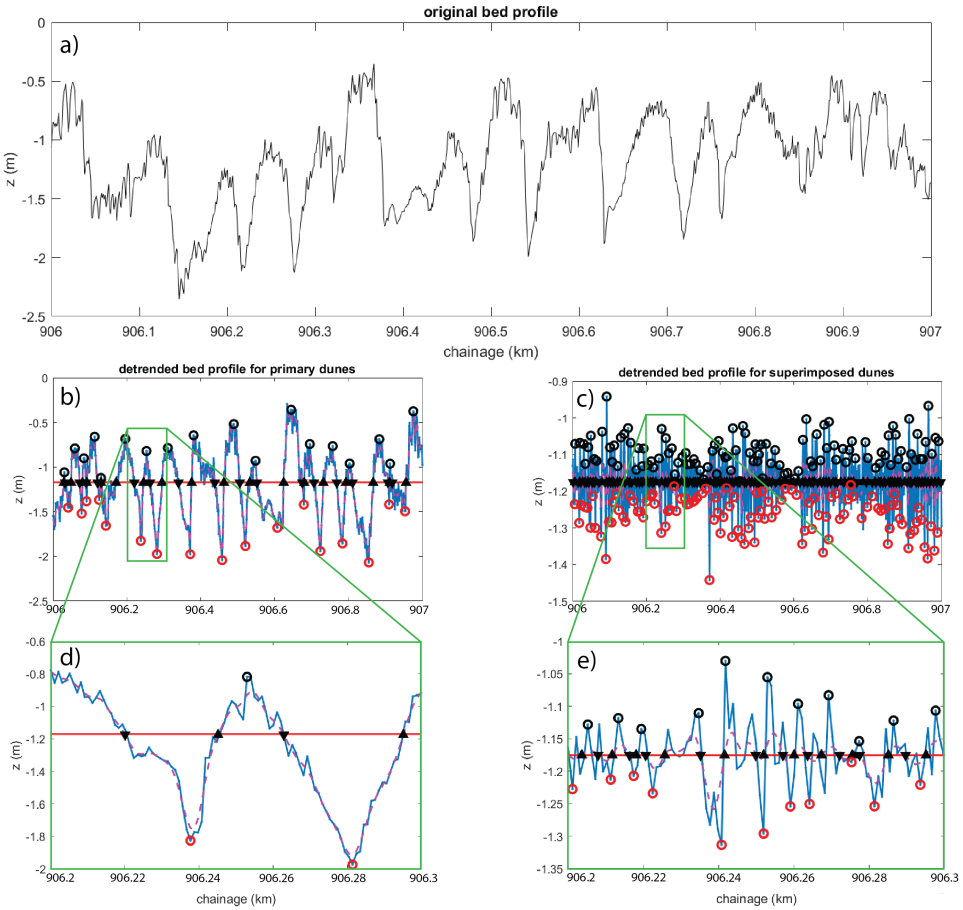

Figure 2. Dune characteristics are defined from the original bed profile (a) using the BTT from Van der Mark and Blom (2007). Detrending and filtering is based on two span values (P0), one for primary dunes (b, d) and one for superimposed bedforms (c, e).

$$k_s = 1.1\gamma_d\Delta(1 - e^{\frac{-25\Delta}{\lambda}}) \tag{4}$$

and γ_d is defined to be equal to 0.7 in field conditions.

Soulsby (1997) used a different formulation of k_s leading to:

$$f_f = \frac{8g}{(18\log(\frac{12d}{30z_0}))^2} \tag{5}$$

in which $z_0 = \Delta^2/\lambda$. Bartholdy et al. (2010) defined k_s in equation 3 as: $k_s = 0.57\ \Delta$

Lefebvre and Winter (2016) developed a new equation based on numerical experiments, including leeside angle, in which form friction is reduced for dunes with a low leeside angle.

$$f_f = \frac{1}{19.75log(\frac{d\lambda}{\Delta^2}) - 20} \tag{6}$$

in which the reduction factor θ is defined as

$$\theta = \frac{1}{1 + e^{-0.2\phi+5.9}} \tag{7}$$

The reduction factor is employed by multiplying it which the form friction factor: $f_{reduced} = f_f\theta$.

The total hydraulic roughness is the sum of form friction, and grain friction (f_g) (Einstein, 1950). Under the assumption that dunes are the fundamental structures causing form resistance, we can now calculate the total hydraulic roughness.

$$f = f_f + f_g \tag{8}$$

Grain roughness is assumed to only depend on grain size distribution and water depth, and is calculated following the approach of Van Rijn (1984).

$$f_g = \frac{8g}{(18log(\frac{12d}{3D_{90}}))^2} \tag{9}$$

in which D_{90} is the 90^{th} percentile of the grain size distribution

3.4 Analysis of leeside angle statistics

We explore if hydraulic roughness variability is correlated to leeside angles, by calculating local topographic leeside angle γ (°) for each square meter in the fairway, based on the two MBES surveys that allow to do so. Hence, we try to infer hydraulic roughness information from MBES data avoiding assumptions about bedforms. If the orientation of a slope in the 1 m x 1 m tile is directed downstream, defined as within ± 30° of the central axis -approximately parallel to the flow direction-, the slope is defined as the leeside.

The MBES data is influenced by side effects such as groynes. To purely focus on the fairway of the river, the groyne influenced part of the river bed is disregarded (Figure 3 and supplementary information Figure S3). To identify the part influenced by groynes, the river is subdivided in sections of 1 km in the streamwise direction, and 1 m in the transverse direction. In these sections, the gradient of the adjacent mean leeside angles is taken and smoothed with a 20 point moving average filter. If at a certain river width

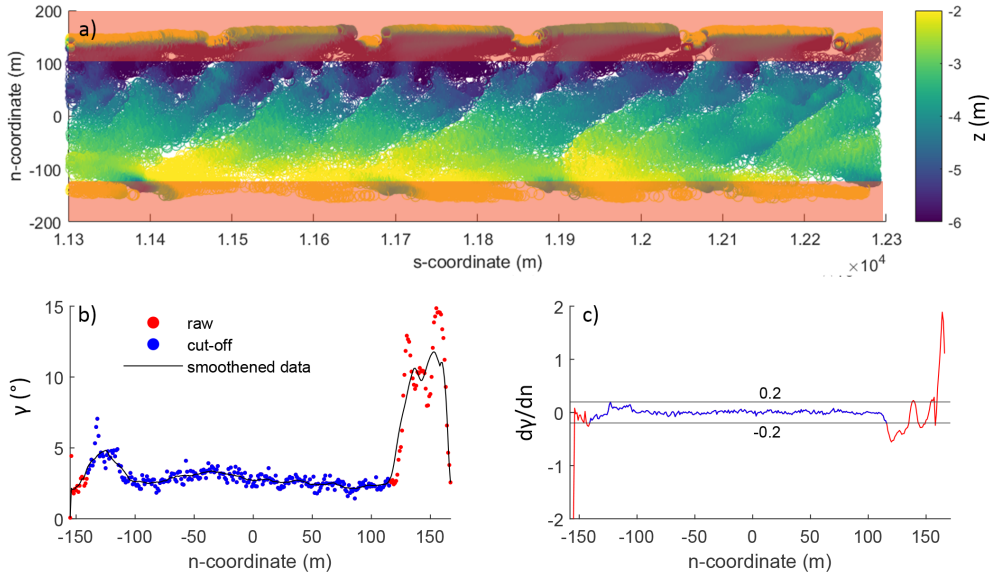

Figure 3. Method to remove the groyne influenced part of MBES data. A: example of a groyne influenced bathymetry, in which the red shaded area is defined as the groyne-influenced part. B: mean leeside angle over the cross-section, averaged per kilometer. C: gradient of the mean local topographic leeside angle. When exceeding three times the standard deviation of the gradient of the mean leeside angle of the middle 100 m of the river (0.19), all data at a larger width is excluded from the analysis (red line).

the gradient is larger than an absolute value of 0.19, all data at a larger width is removed from the analysis. This threshold of 0.19 coincides with 3 times the standard deviation of the gradient of the mean leeside angle in the central 100 m of the river, which is relatively undisturbed by side effects.

The mean local topographic leeside angle γ, calculated from 1 m x 1 m tiles of the river bed, is averaged over the river width and over 1 km along the river. It therefore includes the characteristics of 3D variations in bed geometry of the full width of the non-groyne influenced Waal river bed.

3.5 Coefficient of determination as tool for explaining variance

The coefficient of determination (R^2) shows how much of the variance in hydraulic roughness f is explained by the predictors.

$$R^2 = 1 - \frac{SS_{res}}{SS_{tot}} \tag{10}$$

$$SS_{tot} = \sum_i (f_i - \overline{f})^2 \tag{11}$$

$$SS_{res} = \sum_i (f_i - m_i)^2 \tag{12}$$

in which SS_{tot} is the total sum of squares, SS_{res} the residual sum of squares, f_i the i^{th} observation of f, $\overline{f}$ the mean of the observations f and m_i the i^{th} model prediction output. R^2 will have a value between -1 and 1, indicating the percentage of variability that has been accounted for by the predictor.

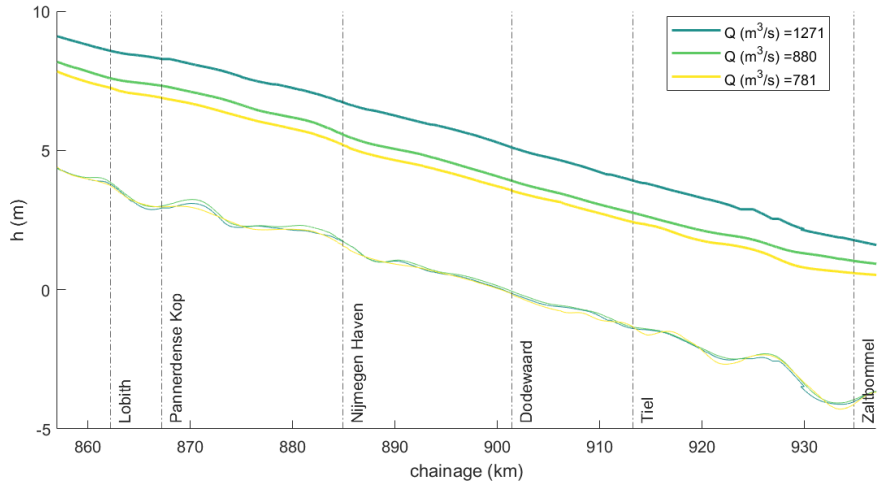

Figure 4. Water surface (thick lines) and bed surface (thin lines) throughout the research for three different discharges.

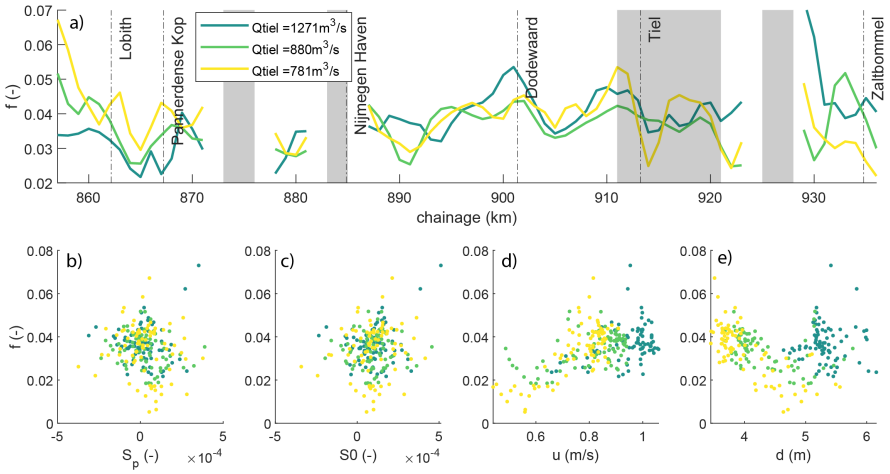

Figure 5. Friction factor f calculated with equation 1 for three different discharges. Shaded grey bars indicate human interference (fixed layers, and longitudinal training dams at Tiel).

4 Results

4.1 Space-time variation in roughness from water level slopes

Figure 4 shows the water surface profiles during the three surveys. Values of f fluctuate between 0.019 and 0.069 (Figure 5). With a mean of 0.035, the River Waal can be characterized as a natural, winding stream (Fetter, 2001). The observed pattern is coherent for different discharges. A lower discharge and correspondingly lower flow velocities, generally result in a higher roughness (f averages 0.037, 0.034, 0.033 $\mathrm{m}^{0.5}s^{-1}$ at a discharge of 1271, 880, 781 m^3s^{-1} respectively). This is especially visible upstream of the Pannerdense Kop, where the Lower Rhine bifurcates in the River Waal and the Pannerdense Kanaal (kanaal means channel). Downstream, this seaming relation between roughness and discharge becomes less clear.

4.2 Roughness predicted from dune geometry

4.2.1 Dune geometry and grain size observations

Grain size changes significantly over the reach subject to study, with a D_{50} ranging from 1 cm upstream to 0.7 mm downstream (Figure 6). This decrease in grain size is reflected in a decrease in grain-related roughness, which is primarily caused by the decrease of D_{90}.

Bedform height averaged per kilometer varies between 0.1 m and 1.5 m, with an average of 0.7 m. Between Lobith and Pannerdense kop, an almost flat bed is observed. Dune height is almost zero in the first 8 kilometers, and increases downstream, but does not exceed 0.7 m (excluding the fixed layer). Relatively constant dune heights, lengths and leeside angles are observed between river kilometre 885 – 915. A similar spatial distribution is observed for both leeside and stoss side angles. The dune geometry is strongly influenced by the fixed layers at Erlecom and Nijmegen. For example, the sine shaped fixed layer in Erlecom is clearly visible in Figure 6, as a deviating length of 50 m and a height of 1.5 m.

Temporal dynamics are less profound. A higher discharge results in higher dunes (on average 0.76 m, 0.82 m, 0.78 m, 0.67 m and 0.58 m between river kilometer 895-936 for Q = 1353, 1271, 1249, 880 and 781 $m^3\ s^{-1}$, respectively), but this does not hold for all locations (Figure 6). No obvious relation between dune height and water depth is found.

Throughout our whole research transect, smaller dunes are imposed on the primary dunes. Those superimposed dunes, or secondary dunes, are on average 0.1 m high and 10 m long, and are clearly distinguishable from the primary dunes being on average 0.7m high and 55m long.

4.2.2 Dune roughness prediction

Predicted values of f follow the same pattern and are in the same order of magnitude as the values of f inferred from the water surface slope (Figure 7). The general trend shown by all predictors reflects a relatively low roughness between Lobith and Pannerdense kop, and an increase in roughness between river km 885-925, followed by a slight decrease until the city of Zaltbommel.

The differences between alternative predictors can reach 0.025. At certain locations, the predicted dune roughness by Bartholdy et al. (2010) is twice higher than the predicted roughness by Lefebvre and Winter (2016). Variations in roughness due to changing discharge conditions are strikingly smaller than differences related to the choice of predictor. Grain size seems to provide an upper limit for the predicted dune roughness values.

Not all variations in roughness inferred from the water surface slopes are captured by the predictions (Figure 8). The coefficient of determination (R^2) shows how much of the variance in f is explained from $f_f + f_g$ for various predictors. For example, R^2 for $f_f + f_g$ predicted with Van Rijn (1984) is 0.43, meaning that 43% of the variability of f has been explained. Alternative predictors exhibit similar trends, yet all other predictors have an R^2 value of less than 0. This means they perform worse than simply taking the average of the roughness inferred from water surface slope data.

4.3 Relation between roughness and leeside angle statistics

The mean local topographic leeside angle is on average 3.5°, which is slightly higher than the mean dune leeside angle (being 2.3°). The distribution of the low topographic leeside angle is highly positively skewed, meaning low angles dominate and higher angles are less frequently occurring.

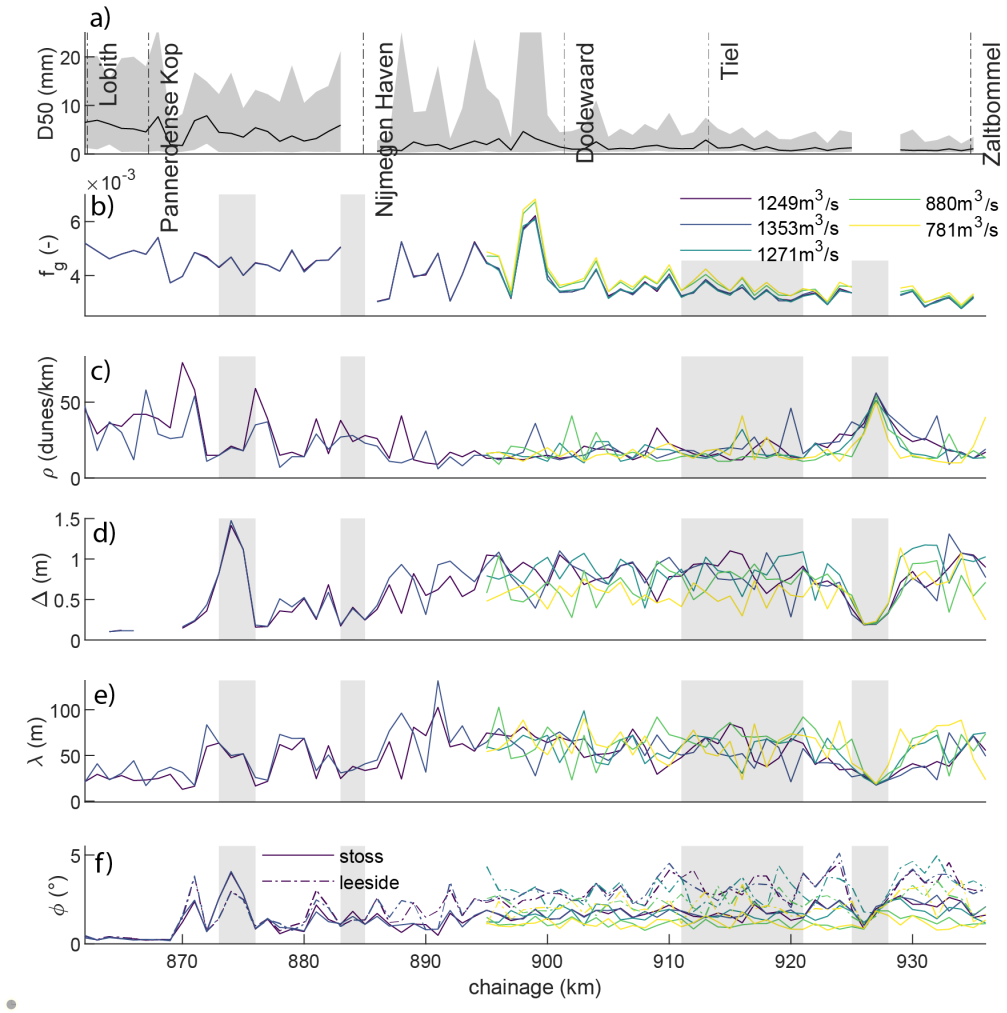

Figure 6. Dune geometry and grain size characteristics. A: Grain size in the research area. Solid line represents D_{50}, the shaded area the D_{10} (lower limit) and D_{90} (upper limit). B: grain roughness, calculated with equation 9, in the research area for various discharges (discharge at Tiel). C: Bedform density (dunes/km), D: mean bedform height, E: man bedform length, F: stoss and leeside angle. Shaded grey bars indicate human interference (fixed layers, and longitudinal training dams at Tiel).

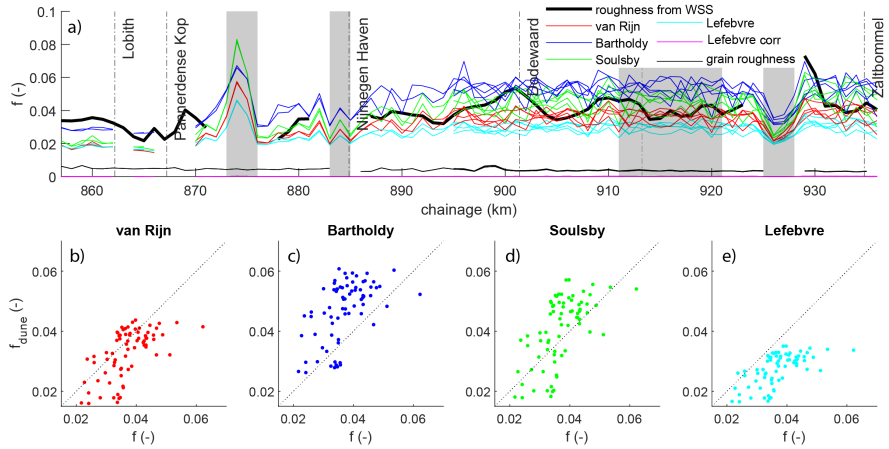

Figure 7. Dune roughness. A: predicted by various predictors (coloured lines) for various discharges (not differentiated). See section 3.3 for corresponding equations. Shaded grey bars indicate human interference (fixed layers, and longitudinal training dams at Tiel). B-E: their relation with roughness calculated with the pressure slope. 'Lefebvre corr' not shown because of severe under prediction.

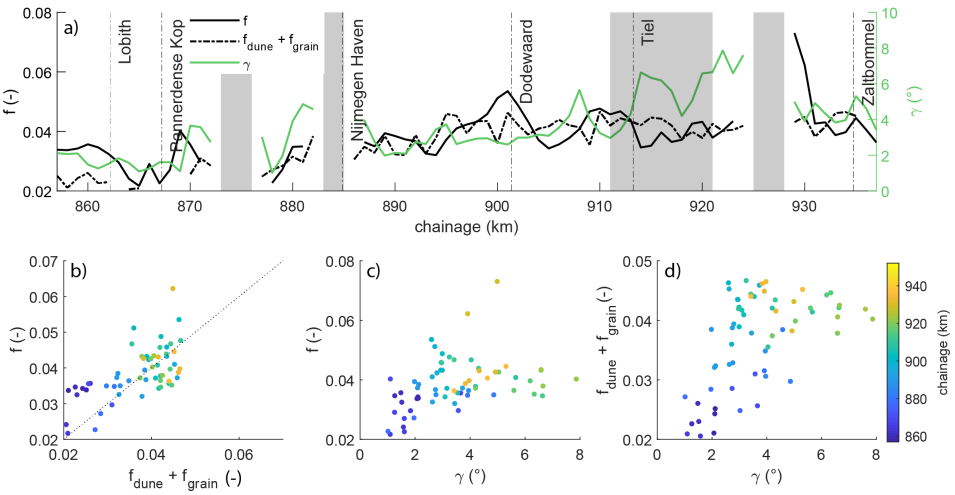

Figure 8. Relation between roughness from water surface slope (f), roughness predicted from dune geometry ($f_{dune} + f_{grain}$) and local topographic leeside angle (γ), against chainage, and their relation with each other. Dune roughness calculated with the predictor of Van Rijn (1984). Compared data comes from different datasets with comparable discharge of Q = 1271 and 1249 $m^3 s^{-1}$. Shaded grey bars indicate human interference (fixed layers, and longitudinal training dams at Tiel).

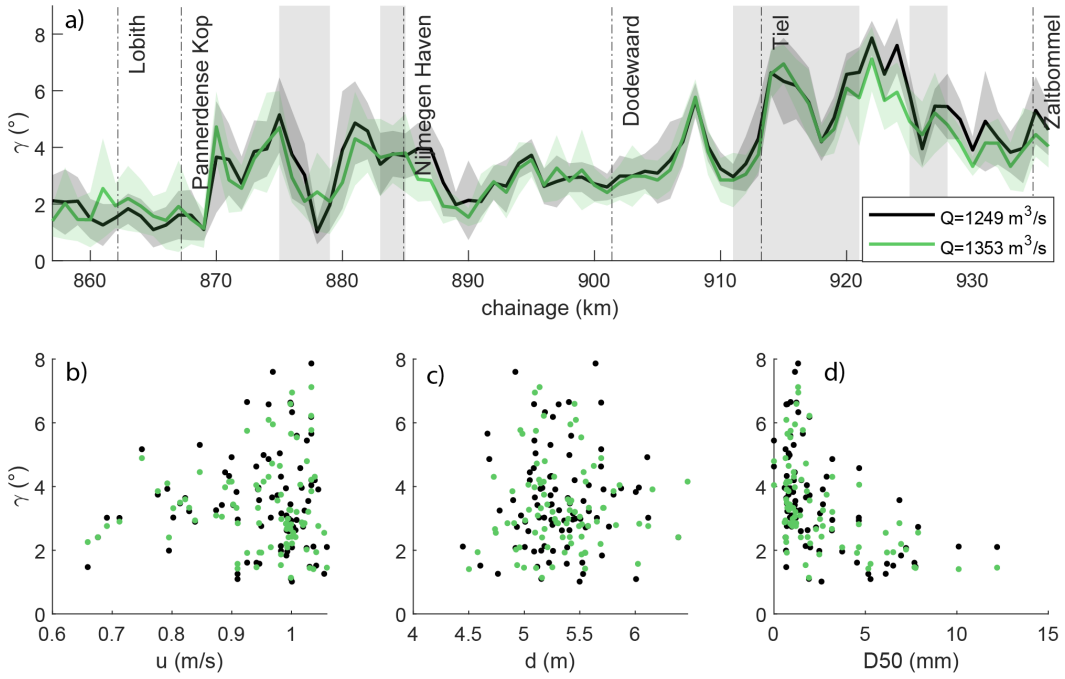

Figure 9. Local topographic leeside angle for two discharges, and its relation with flow velocity, river depth and median grain size. Shaded grey bars indicate human interference (fixed layers, and longitudinal training dams at Tiel).

A very low mean local topographic leeside angle is observed until the Pannerdense Kop (mean 1.7°; Figure 9). Further downstream, the topographic leeside angle slowly increases until Tiel. The trends are comparable for both discharge conditions. Other statistical measures of the local topographic leeside angle follow the same pattern. Mean local topographic leeside angle seems to be unrelated to flow velocity or water depth, and grain size sets an upper limit (Figure 9-B, C, D).

Mean dune leeside angles are lower than local topographical leeside angles. This can indicate that the central axis of the river has lower leeside angles than the sides, which are also included in the measure of local topographic leeside angle. Secondly, the used bedform tracking tool (Van der Mark & Blom, 2007), smooths the bed profile for crest and trough detection, which can cause an underestimation in leeside angle (Zomer et al., 2021). Correlation coefficients (R^2) between γ and f are negative, which contradicts our suspicion that mean leeside angles can better explain effective roughness than roughness predictors based on dunes (Figure 8).

4.4 Influence of depth variation

Since dune predictors explain less than half of the variance of f, it is likely that other roughness imposing elements cause a significant contribution to hydraulic roughness. Figure 10 shows the along river profiles of the detrended bed elevation, width, curvature, transverse bed slope (ξ), detrended streamwise bed elevation gradients (dz_{det}/ds) and the friction coefficient. For consistency, we show figures based on the two most comparable data sets (Q = 1271 $m^3\ s^{-1}$ and 1249 $m^3\ s^{-1}$), and quantify dune roughness with equation 3.

Downstream of river kilometer 893, remarkably, values of f and the gradient in bed elevation show a clear, persistent, out-of-phase relation (Figure 10D). To the authors' knowledge, such relation has never been established before. The downstream stretch is characterized by larger dunes (mean Δ = 0.81m) with a higher leeside angle (mean ϕ = 3.0°, mean γ = 4.4°), a comparatively small difference between hydraulic roughness and the roughness predicted based on dune geometry ($f_{dune} - f_{grain}$ = 0.005, and R^2 between f and $f_{dune} - f_{grain}$) = 0.39), a smaller standard deviation in smoothed detrended bed level (std z = 0.1) and a negative correlation between f and dz/ds (corr = -0.67, see Figure 11).

The observed anti-phase relation can be understood intuitively and is summarized in Figure 12. When the flow approaches a shallow part of the river along the transect (dz_{det}/ds decreases), the roughness increases, and vice versa, towards a deeper part (dz_{det}/ds increases), the friction coefficient decreases. An increase of the water depth will cause the flow to diverge and decelerate. The resulting energy losses manifest as an increased value of f are not directly related to bed roughness, but rather a result of depth increase, analogous to the widening section of a Venturi meter. The normalized values of gradient in bed level and roughness have a coefficient of correlation of 0.34, which means that the inverse gradient in bed elevation explains 34% of the variability in roughness.

Upstream of river kilometer 893, the out-of-phase relation between dz_{det}/ds and f is lost. This reach is characterized by low dunes (mean Δ = 0.3m) with a low leeside angle (mean ϕ = 1.2°, mean γ = 2.4°), a large difference between the hydraulic roughness and roughness predicted based on dune geometry (f - $f_{dune} - f_{grain}$ = 0.01, R^2(f, $f_{dune} - f_{grain}$) = 0.26), a large standard deviation in smoothed, detrended bed level (std z = 0.2) (Figure 11). This is a highly complicated reach, with coarse sediment and large fluctuations in grain size (Figure 6), impacts of fixed layers, and strong curvature (Figure 10).

5 Discussion

The observed counter-phase fluctuation of the detrended bed elevation gradient and the friction coefficient (Figure 10-D) occurs on a slightly larger spatial scale than alternating bars, which are clearly imposed by channel curvature (Figure 10-C). Large scale fluctuations of the river depth are found all around the world in studies demonstrating river geometrical variation (Venditti et al., 2019; Trigg et al., 2009; Leuven et al., 2021; Gallo & Vinzon, 2005), and are often related to stratigraphy. The counter-phase relation may partly depend on the smoothing, which results from spatial filtering. Smoothing has significant consequences both for the resulting bed slope (Figure 13) and for values of f. In this study, the choice of filtering was motivated by a spectral gap between bed level variations by bedforms, including dunes, and regional scale variations imposed by the geological setting, human-made constraints such as groynes, and alternate bars. Whereas we expected that part of the variance of f could be explained by each of the latter factors, serendipitously, we found a clue that along-river variation of the depth can have a significant impact on the effective roughness.

Although the along-river variation of the elevation gradients holds a much stronger relation to the friction factor f than alternate bars, the observed point bars in the River Waal can exert an indirect control on hydraulic roughness, which extends beyond the impact on dune properties (de Ruijsscher et al., 2020). Flow concentrates in the deepest part of the river, opposite to bars, as shown in Zomer et al. (2021). The resulting variation in flow velocity over the cross-section is significant, which means that for a uniform bedform field the effective roughness can vary over the cross-section. Consequently, considering the nonlinearity of roughness relations, width-averaged properties of dunes may not be entirely representative. Width variations as visible in Figure 10B can further complicate the planimetric flow structure, causing the flow to converge or diverge.

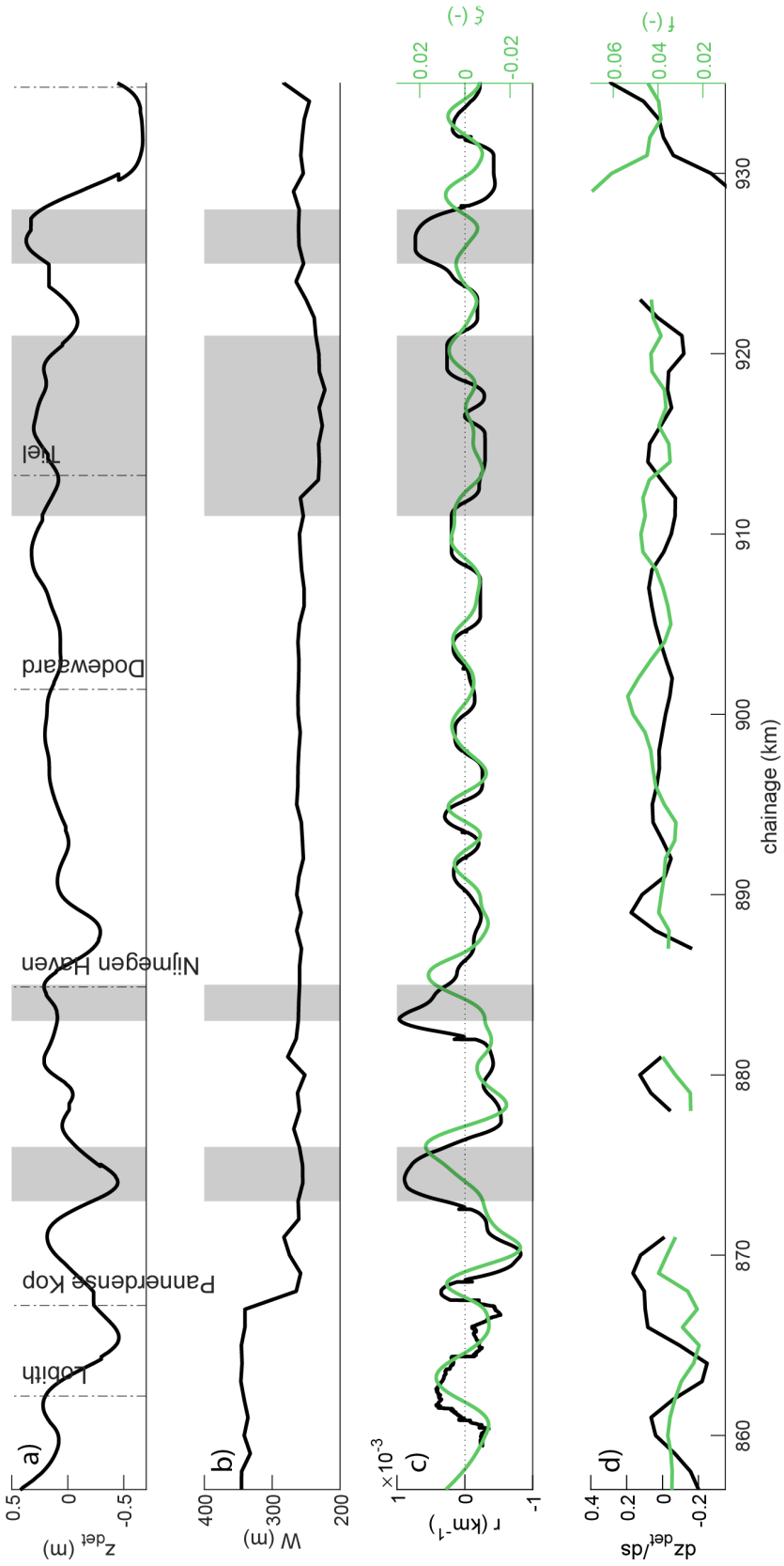

Figure 10. River geometry, curvature and hydraulic roughness, from datasets with comparable discharges (Q = 1271 and 1249 $m^3 s^{-1}$). Shaded grey bars indicate human interference (fixed layers, and longitudinal training dams at Tiel). A: bed level, detrended with a third degree polynomial and smoothed with a 8km loess filter, B: river width, C: river curvature (black) and transverse bed slope ξ (green), D: roughness calculated with the pressure slope (green) and gradient of detrended bed level (z_{det}; black).

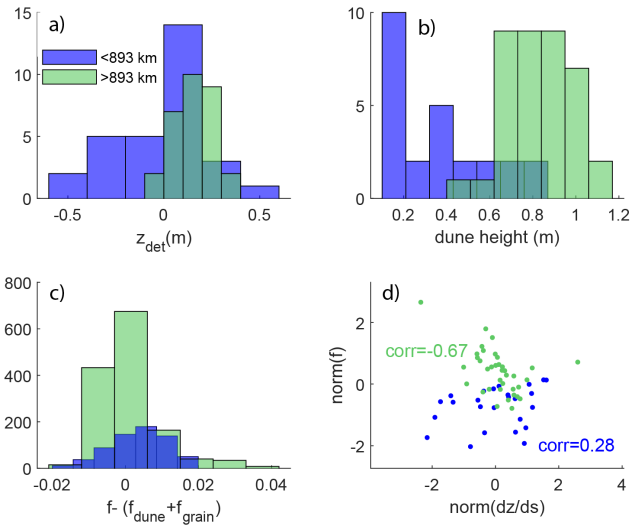

Figure 11. Histograms of various river characteristics, divided in upstream and downstream of river kilometer 893. A: Detrended bed level, B: dune height C: the difference between roughness calculated with the pressure slope and with predictors based on dune geometry. D: normalized gradient of detrended bed level against normalized roughness, with a different Pearson's correlation coefficient (Pearson, 1909) upstream and downstream of river kilometer 893 (corr = 0.28 and -0.67 respectively).

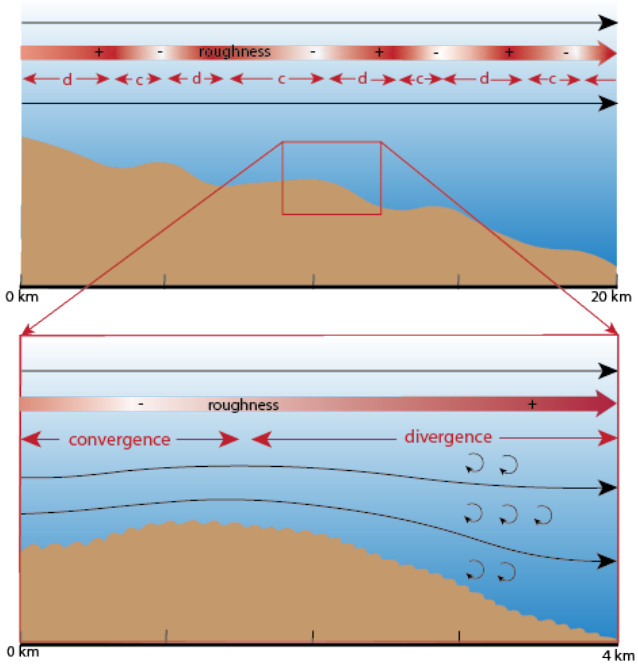

Figure 12. Graphical representation of the hypothesis how large scale fluctuations of bed slope can influence hydraulic roughness. Low and high values of roughness (marked with + and - signs), and convergence (c) and divergence (d) zones of the water flow are indicated.

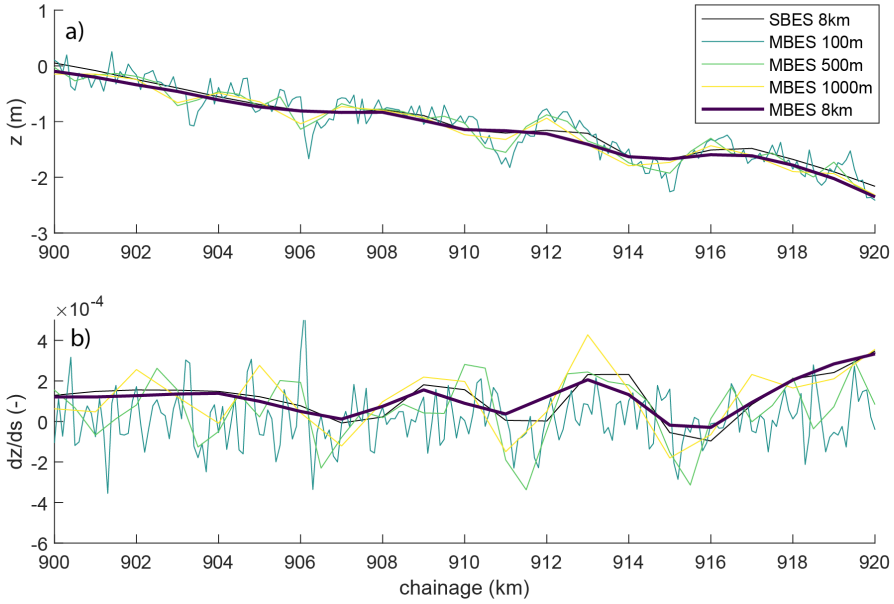

Figure 13. The influence of the choice of data input and the degree of smoothing on bed level and the corresponding bed slope. Input data is either a single profile (SBES) or width-averaged (MBES) and smoothed with a loess filter of various degrees. When choosing a filtering of 8 km, both types of input data generate the same bed slope.

In our research area, width variations are small and gradual (except for the bifurcation at Pannerdense Kop, where the Rhine bifurcates in the river Waal and Pannerdense Kanaal).

The leeside angles observed in our study domain are low, which is common in large rivers (Galeazzi et al., 2018; Hendershot et al., 2016; Cisneros et al., 2020). The mean leeside angle per kilometre does not exceed 5°. Low-angle dunes generate less turbulence than dunes with permanent flow separation (Cisneros et al., 2020), which can be accounted for in roughness predictions (Lefebvre & Winter, 2016). The slip face of dunes, the steepest part of the leeside angle, is considered to be important, as the size of the flow separation zone relates to the height of the slip face crest (Paarlberg et al., 2007). Kornman (1995) found that form roughness is better quantified using the height of the slip face angle than bedform height. Against expectations, mean local topographic leeside angles of low-angled dunes explain little of the observed roughness variations. Attempts to explain the observed roughness variation from alternative statistics of dune leeside angle, such as all angles higher than 14°, were unsuccessful. Hard evidence that the detailed shape of dunes matters, beyond properties that are included in classical roughness predictors such as the one from Van Rijn (1984), is lacking.

Secondary dunes are sometimes considered to be a separate roughness element (Julien et al., 2002), resulting in f = $f_p + f_s + f_g$ (roughness from primary dunes, secondary dunes and grains, respectively). Taking the roughness predictor from Van Rijn (1984) as an example, roughness contribution from secondary dunes to f is on average 0.022, while the contribution from primary dunes is 0.034. Adding roughness from primary and secondary dunes together following the above mentioned equation, leads to an overestimation of hydraulic roughness by almost 100%. This overestimation is caused by the fact that primary and secondary dunes are not two separated roughness elements, but are superimposed on each other and have a joint effect on the flow dynamics. The pres-

ence of superimposed dunes will presumably increase the imposed form roughness, and quantification of this effect is a topic for further research.

The grain size distribution on the Lower Rhine and River Waal shows a clear pattern of downstream fining. The grain roughness decreases in downstream direction, but the contribution of grain roughness to the total roughness is low. The grain size distribution does impact the potential for dune formation and growth (van den Berg & van Gelder, 1993), and in such a way that in the Lower Rhine dunes only form under high discharges (Wilbers & Ten Brinke, 2003). Dunes found under lower discharges can be remnants of former high flow conditions. Grain size can also vary over the cross-section. The passage of heavy ships induces erosion of the fine-grained beaches between the groynes, resulting into transport of fine-grained sand to the river bed (Wilbers & Ten Brinke, 2003). The currents induced by ships are stronger moving upstream (Bhowmik et al., 1995). Therefore, the southern side of the River Waal will be subject to more fine sand input. The implications of this difference in grain size over cross-section on dune geometry remains to be explored.

Resistance by groynes contribute to the total hydraulic roughness of the channel. Groynes are known to cause turbulence and therefor scour behind the groyne heads, and locally, the river bed can show undulations with the same wave length as the groyne spacing (Wilbers & Ten Brinke, 2003). Those undulations are fixed and do not interact with bedforms (Wilbers, 1999; Ouillon & Dartus, 1997), but could statically influence bedform geometry (de Ruijsscher et al., 2020). The influence of groynes change with higher discharge conditions, especially when groynes will be submerged and become part of the conducting section of the bed (Möws; & Koll, 2019; Yossef, 2004). The ubiquitous presence of groynes along both banks makes it impossible to quantify groyne roughness in this study, also because the expected undulations in the water surface profile are too subtle to be observed based on ship positioning. High resolution measurements of the water surface topography, which cover the full width of the river instead of merely a single track along the center line of river, may further elucidate the causes of hydraulic roughness variation required in models simulating flow, sediment transport and bed morphological change.

6 Conclusions

We quantified hydraulic roughness based on the Darcy-Weisbach friction factor calculated from hydraulic field data of a 78 km long trajectory of the Lower Rhine and River Waal in the Netherlands. This was compared to predicted roughness values based on dune geometry, and to the spatial distribution of the local topographic leeside angle, both inferred from bathymetric field data.

In the upstream part of the river trajectory subject to study, where dunes are likely inactive under low flow conditions and human-made hard layers cause nonuniform flow, total hydraulic roughness cannot be easily predicted from bedform dimensions. In the downstream part, predictions of the Darcy-Weisbach friction factor f agree with estimates inferred from longitudinal surface level profiles. The best performing predictor explains 42% of the variance in f, which indicates that even in this part of the river, dune morphology is not the only factor explaining hydraulic roughness variation. We expected to explain part of the variance in f from statistics of local leeside bed level gradients, which control flow separation and energy loss, but did not find confirmation of this expectation. Alternatively we found that longitudinal profiles of the gradient of smoothed river bed level, oscillates in counter phase with f. Towards a topographic high, the friction factor decreases, and towards a topographic low, the friction factor increases. A deepening of the river thus corresponds with a higher hydraulic roughness, which may relate to flow divergence in the decelerating flow, and the corresponding energy loss. The depth variations explain 34% of the variance in hydraulic roughness. This effect is clearly vis-

ible in the downstream region, where the grain size is relatively constant, dunes are comparatively large, and dune predictors explain a large part of the variance in f. Unresolved influences on hydraulic roughness include the effect of man-made structures such as groynes, secondary-dunes and topographical steering of the river flow. Future work to further elucidate the effect of complex bed geometry, -both small (secondary dunes) and large scale-, on hydraulic roughness is warranted.

Appendix A Derivation of st. Venant equation

The momentum balance of the St.-Venant equations expressed in water level and velocity reads:

$$\frac{\partial u}{\partial t} + u\frac{\partial u}{\partial s} + gS_p = g(S_0 - S_f) \tag{A1}$$

where u = depth and cross-sectional averaged flow velocity (Q/A, m/s), where Q = discharge ($m^3\ s^{-1}$) and A = wetted area (m^2), S_p = pressure slope (= $\frac{\partial d}{\partial s}$, where d is hydraulic depth), S_0 = bottom slope (= $\frac{\partial z}{\partial s}$, where z = bed level relative to Amsterdam Ordnance Datum, m), and

$$S_f = \frac{Q^2}{C^2A^2R} \tag{A2}$$

in which C = Chézy coefficient ($m^{1/2}\ s^{-1}$), and R = hydraulic radius (m). Assuming R $\approx$ d, which applies to lowland rivers for which $W \gg d$, equation A3 can be simplified as:

$$S_f = \frac{u^2}{C^2d} \tag{A3}$$

For the lowland river subject to study the time derivative term is two orders of magnitude smaller than other terms in the momentum equation, so we set $\frac{\partial u}{\partial t} \approx 0$. After rewriting, Chézy coefficient can be obtained as:

$$C = \frac{u}{\sqrt{d(S_0 - S_p - \frac{\partial Qu}{\partial s}\frac{1}{gA})}} \tag{A4}$$

Acronyms

BTT Bedform Tracking Tool
MBES Multibeam Echosounder
SBES Singlebeam Echosounder
RWS Rijkswaterstaat, Dutch Ministry for Infrastructure and Environment
NAP Amsterdam Ordnance Datum
ADCP Acoustic Doppler Current Profiler
LTDs longitudinal training dams
RMSE root mean square error

Acknowledgments

This research was funded by the Netherlands Organisation for Scientific Research (NWO), within Vici project "Deltas out of shape: regime changes of sediment dynamics in tide-

influenced deltas" (Grant NWO-TTW 17062). We would like to thank Rijkswaterstaat, the Dutch Ministry for Infrastructure and Environment, for providing the data. Furthermore Arjan Sieben and Denes Beyer from Rijkwaterstaat provided helpful feedback on the data analysis and interpretation. (Anonymous) reviewers will be thanked. Data will be made publicly available via https://doi.org/10.4121/c.5405382.

References

Bartholdy, J., Flemming, B. W., Ernstsen, V. B., Winter, C., & Bartholomä, A. (2010). Hydraulic roughness over simple subaqueous dunes. *Geo-Marine Letters*, *30*(1), 63–76. doi: 10.1007/s00367-009-0153-7

Best, J., & Kostaschuk, R. (2002). An experimental study of turbulent flow over a low-angle dune. *Journal of Geophysical Research C: Oceans*, *107*(9), 18–1. doi: 10.1029/2000jc000294

Bhowmik, B. N. G., Xia, R., Member, A., Mazumder, B. S., & Soong, T. W. (1995). Return flow in rivers due to navigation traffic. *Journal of Hydraulic Engineering*, *121*(12), 914–918.

Buschman, F. A., Hoitink, A. J., Van Der Vegt, M., & Hoekstra, P. (2009). Subtidal water level variation controlled by river flow and tides. *Water Resources Research*, *45*(10), 1–12. doi: 10.1029/2009WR008167

Chow, V. (1959). *Open-channel hydraulics*. McGraw-Hill Book Company, USA.

Cisneros, J., Best, J., van Dijk, T., Almeida, R. P. d., Amsler, M., Boldt, J., ... Zhang, Y. (2020). Dunes in the world's big rivers are characterized by low-angle lee-side slopes and a complex shape. *Nature Geoscience*, *13*(2), 156–162. doi: 10.1038/s41561-019-0511-7

Cleveland, W. (1979). Robust local weighted regression and smoothing scatterplots. *of the American Statistical Association*, *74*(368), 829–836.

Cleveland, W., & Devlin, S. (1988). Weighted regression: an approach to regression analysis by local fitting. *Journal of the American Statistical Association*, *83*(403), 596–610.

de Ruijsscher, T., Hoitink, A., Dinnissen, S., Vermeulen, B., & Hazenberg, P. (2018). Application of a Line Laser Scanner for Bed Form Tracking in a Laboratory Flume. *Water Resources Research*, *54*(3), 2078–2094. doi: 10.1002/2017WR021646

de Ruijsscher, T., Naqshband, S., & Hoitink, A. (2020). Effect of non-migrating bars on dune dynamics in a lowland river. *Earth Surface Processes and Landforms*.

Einstein, H. A. (1950). The bed-load function for sediment transportation in open channel flows. *Technical Bulletins 156389, United States Department of Agriculture, Economic Research Service.*.

Engelund, F., & Hansen, E. (1967). Monograph on Sediment Transport. *Technisk Forlag, Copenhagen, Denmark*.

Fetter, C. (2001). *Applied Hydrogeology* (4th ed.). New Jersey: Prentice Hall.

Galeazzi, C. P., Almeida, R. P., Mazoca, C. E., Best, J. L., Freitas, B. T., Ianniruberto, M., ... Tamura, L. N. (2018). The significance of superimposed dunes in the Amazon River: Implications for how large rivers are identified in the rock record. *Sedimentology*, *65*(7), 2388–2403. doi: 10.1111/sed.12471

Gallo, M. N., & Vinzon, S. B. (2005). Generation of overtides and compound tides in Amazon estuary. *Ocean Dynamics*, *55*(5-6), 441–448. doi: 10.1007/s10236-005-0003-8

Gates, T., & Al-Zahrani, M. (1996). Spatiotemporal stochastic open-channel flow. II: simulation experiments. *Journal of Hydraulic Engineering*, *122*(11), 652–611. doi: 10.1061/(ASCE)07339429(1996)122:11(652).

Hendershot, M. L., Venditti, J. G., Bradley, R. W., Kostaschuk, R. A., Church, M., & Allison, M. A. (2016). Response of low-angle dunes to variable flow. *Sedimentology*, *63*(3), 743–760. doi: 10.1111/sed.12236

Hidayat, H., Vermeulen, B., Sassi, M. G., F. Torfs, P. J., & Hoitink, A. J. (2011). Discharge estimation in a backwater affected meandering river. *Hydrology and Earth System Sciences*, *15*(8), 2717–2728. doi: 10.5194/hess-15-2717-2011

Hoitink, A. J., Buschman, F. A., & Vermeulen, B. (2009). Continuous measurements of discharge from a horizontal acoustic Doppler current profiler in a tidal river. *Water Resources Research*, *45*(11), 1–13. doi: 10.1029/2009WR007791

Julien, P. Y., Klaassen, G. J., Ten Brinke, W. B., & Wilbers, A. W. (2002). Case study: Bed resistance of Rhine River during 1998 flood. *Journal of Hydraulic Engineering*, *128*(12), 1042–1050. doi: 10.1061/(ASCE)0733-9429(2002)128:12(1042)

Klemes, V. (1986). Operational testing of hydrological simulation models. *Hydrological Sciences Journal*, *31*(1), 13–24. doi: 10.1080/02626668609491024

Kornman, B. (1995). *The effect of changes in the lee shape ofdunes on the flow field, turbulence, and hydraulic roughness* (Tech. Rep.). Utrecht: University of Utrecht.

Kostaschuk, R. A., & Venditti, J. G. (2019). Why do large, deep rivers have low-angle dune beds? *Geology*, *47*(10), 919–922. Retrieved from `https://doi.org/10.1130/G46460.1` doi: 10.1130/G46460.1

Lefebvre, A., Ernstsen, V. B., & Winter, C. (2013). Estimation of roughness lengths and flow separation over compound bedforms in a natural-tidal inlet. *Continental Shelf Research*, *61-62*, 98–111. doi: 10.1016/j.csr.2013.04.030

Lefebvre, A., & Winter, C. (2016). Predicting bed form roughness: the influence of lee side angle. *Geo-Marine Letters*, *36*(2), 121–133. doi: 10.1007/s00367-016-0436-8

Leuven, J., van Keulen, D., Nienhuis, J., Canestrelli, A., & Hoitink, A. (2021). Large-scale scour in response to tidal dominance in estuaries. *Journal of Geophysical research: Earth surface*, *conditiona*.

Möws;, R., & Koll, K. (2019). Roughness E ect of Submerged Groyne Fields with Varying Length, Groyne Distance, and Groyne Types. *Water*, *11*(1253). doi: 10.3390/w11061253

Ouillon, S., & Dartus, D. (1997). Three-dimensional computation of flow around groyne. *Journal of Hydraulic Engineering*, *123*(11).

Paarlberg, A. J., Dohmen-Janssen, C. M., Hulscher, S. J., & Termes, P. (2007). A parameterization of flow separation over subaqueous dunes. *Water Resources Research*, *43*(12), 1–10. doi: 10.1029/2006WR005425

Pearson, E. S. (1909). Determination of the Coefficient of Correlation. *Science*, *30*(757), 23–25.

Reneerkens, M. (2020). *De bodemsamenstelling van de Rijntakken in de jaren 1995 en 2020* (Tech. Rep.). RWS ON rapport.

Ruijsscher, T. V. D., Hoitink, A. J. F., Naqshband, S., & Paarlberg, A. J. (2019). Bed morphodynamics at the intake of a side channel controlled by sill geometry. *Advances in Water Resources*, *134*(February). doi: 10.1016/j.advwatres.2019.103452

RWS-WVL, & Deltares. (2017). *Beschrijving Modelschematisatie Rijn 5e-generatie Baseline, WAQUA en SOBEK3* (Vol. 01; Tech. Rep.).

Sassi, M. G., Hoitink, A. J., De Brye, B., Vermeulen, B., & Deleersnijder, E. (2011). Tidal impact on the division of river discharge over distributary channels in the Mahakam Delta. *Ocean Dynamics*, *61*(12), 2211–2228. doi: 10.1007/s10236-011-0473-9

Schielen, R. M., Jesse, P., & Bolwidt, L. J. (2007). On the use of flexible spillways to control the discharge ratio of the Rhine in the Netherlands. *Geologie en Mijnbouw/Netherlands Journal of Geosciences*, *86*(1), 159. doi: 10.1017/S0016774600023155

Sieben, A. (2020). *Overzicht afvoermetingen 2016-2019 project monitoring langsdammen* (Tech. Rep.).

Silberman, E., Carter, R., Einstein, H., Hinds, J., Powell, R., & Channels, A. T. F. o. F. F. i. O. (1963). Friction factors in open channels. *J. Hydraul. Eng.*, *89*(HY2), 97–143.

Sloff, C. J., Mosselman, E., & Sieben, J. (2006). Effective use of non-erodible layers for improving navigability. *Proceedings of the International Conference on Fluvial Hydraulics - River Flow 2006*, *2*, 1211–1220. doi: 10.1201/9781439833865.ch127

Soulsby, R. (1997). *Dynamics of marine sands.* London, Thomas Telford, 249p.

Trigg, M. A., Wilson, M. D., Bates, P. D., Horritt, M. S., Alsdorf, D. E., Forsberg, B. R., & Vega, M. C. (2009). Amazon flood wave hydraulics. *Journal of Hydrology*, *374*(1-2), 92–105. doi: 10.1016/j.jhydrol.2009.06.004

van den Berg, J., & van Gelder, A. (1993). A new bedform stability diagram, with emphasis on the transiton of ripples to plane bed in flows over fine sand and silt. *Spec. Publs Int. Ass. Sediment*, *17*, 11–21.

Van der Mark, C. F., & Blom, A. (2007). *A new and widely applicable tool for determining the geometric properties of bedforms* (Tech. Rep.). University of Twente.

Van Rijn, L. (1984). Sediment transport, part III: Bedforms. *Journal of Hydraulic Engineering*, *110*(12), 1733–1754.

Venditti, J., Nittrouer, J., Allison, M., Humphries, R., & Church, M. (2019). Supply-limited bedform patterns and scaling downstream of a gravel–sand transition. *Sedimentology*, *66*(6), 2538–2556. doi: 10.1111/sed.12604

Vermeulen, B., Hoitink, A. J., & Sassi, M. G. (2013). On the use of horizontal acoustic Doppler profilers for continuous bed shear stress monitoring. *International Journal of Sediment Research*, *28*(2), 260–268. doi: 10.1016/S1001-6279(13)60037-2

Vermeulen, B., Hoitink, A. J., Van Berkum, S. W., & Hidayat, H. (2014). Sharp bends associated with deep scours in a tropical river: The river Mahakam (East Kalimantan, Indonesia). *Journal of Geophysical Research: Earth Surface*, *119*(7), 1441–1454. doi: 10.1002/2013JF002923

Warmink, J. J. (2011). *Unraveling uncertainties.* Retrieved from `http://purl.org/utwente/doi/10.3990/1.9789036532273` doi: 10.3990/1.9789036532273

Warmink, J. J., Booij, M. J., Van der Klis, H., & Hulscher, S. J. (2013). Quantification of uncertainty in design water levels due to uncertain bed form roughness in the Dutch river Waal. *Hydrological Processes*, *27*(11), 1646–1663. doi: 10.1002/hyp.9319

Wilbers, A. (1999). Bed Load Transport and Dune Development Of, in the Rhine: Echo-soundings from the Flood November 1998 (in Dutch). *ICG Report 99/10. ICG, Utrecht University, Utrecht*.

Wilbers, A., & Ten Brinke, W. (2003). The response of subaqueous dunes to floods in sand and gravel bed reaches of the Dutch Rhine. *Sedimentology*, *50*(6), 1013–1034. doi: 10.1046/j.1365-3091.2003.00585.x

Yossef, M. (2004). The effect of the submergence level on the resistance of groynes - an experimental investigation. In *The 6th int. conf. on hydroscience and engineering (iche-2004).*

Zomer, J. Y., Naqshband, S., Vermeulen, B., & Hoitink, A. J. F. (2021). Rapidly migrating secondary bedforms can persist in the lee of slowly migrating primary river dunes. *JGR Earth Surface*, 1–20. doi: 10.1029/2020JF005918